AIAA AVIATION Forum
17-21 June 2019, Dallas, Texas
AIAA Aviation 2019 Forum

10.2514/6.2019-2885

Check for updates

Integrated Sizing and Optimization of Hybrid Wing Body Aircraft in Conceptual Design

Jiacheng Xie*, Yu Cai†, Mengzhen Chen‡, and Dimitri N. Mavris§
Aerospace Systems Design Laboratory, School of Aerospace Engineering
Georgia Institute of Technology, Atlanta, Georgia, 30332

The hybrid wing body (HWB) configuration is a paradigm shift in commercial transport aircraft design in terms of environmentally responsible characteristics and significant performance improvements over the conventional tube-and-wing configuration. However, the sizing methods and analysis tools used in conceptual design of tube-and-wing aircraft are not fully compatible with HWB due to the highly integrated fuselage and wing. This paper proposes a novel approach to perform parametric sizing and optimization of HWB aircraft at the conceptual design phase, and develops an interdisciplinary design framework which integrates preliminary aerodynamic analysis, weight estimation, propulsion system sizing, and mission analysis. Enabled by the techniques of Design of Experiments and surrogate modeling, a design space exploration is conducted over the top-level aircraft design variables, including sensitivity assessment, feasible design space identification, and constrained multi-objective optimization. The impact of uncertainties in disciplinary analyses and novel technologies on aircraft-level performance is investigated through an uncertainty analysis.

I. Introduction

Future commercial aircraft are expected to perform environment-friendly and highly fuel-efficient. In NASA Environmentally Responsible Aviation (ERA) project [1], a set of time-frame goals for next-generation transport aircraft in terms of environmental impacts and performance improvements are defined for future subsonic commercial transport, as presented in Table 1. To achieve these strict design requirements, novel configurations are surged with great interests, since the conventional tube-and-wing configuration is unlikely to satisfy these improvement targets. The hybrid wing body (HWB) configuration, also known as the blended wing body (BWB), is one of these novel configurations for transport aircraft. This configuration is attractive to future commercial aircraft designers due to the higher aerodynamic efficiency over conventional aircraft owing to geometrically integrated wing and fuselage, which leads to potential reduction in noise, emissions, fuel consumption, and improvements in flight performance [2].

Table 1 NASA ERA Subsonic Transport System Level Metrics Targets [1]

Metrics	N+1 (2015) Conventional Tube and Wing (relative to B737/CFM56)	N+2 (2020) Unconventional HWB (relative to B777/GE90)	N+3 (2030-2035) Advanced Aircraft Concepts
Noise	−32 dB	−42 dB	55 LDN (dB)
LTO NOx Emissions (below CAEP 6)	−60%	−75%	Better than −75%
Fuel Burn	−33%	−40%	Better than −70%
Field Length	−33%	−50%	Exploit Metroplex Concepts

With the surge in HWB interest, numerous studies on HWB designs have been performed in academia and industry. Past studies have focused on the disciplinary analysis for HWB, including geometry and configuration

*Graduate Researcher, ASDL, School of Aerospace Engineering, Georgia Tech, AIAA Student Member
†Graduate Researcher, ASDL, School of Aerospace Engineering, Georgia Tech, AIAA Student Member
‡Graduate Researcher, ASDL, School of Aerospace Engineering, Georgia Tech, AIAA Student Member
§S.P. Langley Distinguished Regents Professor and Director of ASDL, Georgia Tech, AIAA Fellow

Copyright © 2019 by Jiacheng Xie, Yu Cai, Mengzhen Chen, and Dimitri N. Mavris. Published by the American Institute of Aeronautics and Astronautics, Inc., with permission.

modeling [3–5], aerodynamics [6–8], structure [9–11], propulsion [12], emission and noise [13], control surface layout and actuation [2, 14, 15], and subsystems sizing [16], etc. However, while the methodologies of conventional tube-and-wing aircraft sizing have been widely addressed in articles and textbooks [17, 18], it has rarely been discussed how HWB should be sized and optimized based on point performance and mission performance requirements. The research objective of this study is to propose an integrated approach for HWB aircraft conceptual sizing and optimization. The multi-fidelity conceptual sizing approach incorporates disciplinary analyses using both physics-based and semi-empirical methods, an integrated mission analysis algorithm, and top-level design parameters which are re-defined to be compatible with HWB geometry. The surrogate modeling technique is widely used in the overall sizing and optimization process to facilitate design space exploration.

The remainder of this paper is organized as follows: Section II provides a summary overview of the sizing and optimization process; Section III introduces the multi-fidelity approach used in major disciplinary analyses; Section IV discusses the selection of design variables and the baseline aircraft; Section V presents the design space exploration conducted over design variables; Section VI evaluates the impact of uncertainties on sizing and optimization process; finally, Section VII draws the conclusion.

II. Overall Sizing and Optimization Process

The integrated sizing and optimization process for HWB aircraft is briefly described as follows.

1) **Problem definition:** This step defines the top-level aircraft requirements and metrics of interest, which are selected based on the "N+2" target performance improvements in Table 1, including takeoff field length (TOFL), landing field length (LFL), approach speed (VAPP), block fuel (BF), operating empty weight (OEW), and ramp weight (RW). Noise and NOx emission are not considered at this stage due to lack of access to analysis tool.
2) **Baseline aircraft identification:** This step identifies a notional HWB baseline aircraft for the optimization task. Since there does not exist a single type of HWB in commercial service which can be used for calibration, the development of baseline has to rely on published HWB models such as NASA N2A [19], Boeing BWB-0009A [20], and NASA/Boeing ERA-224 [21], etc.
3) **Design space definition:** In this step, a group of independent top-level aircraft parameters are identified as the design variables. A Design of Experiments (DoE) is then prepared based on their assigned ranges.
4) **Modeling and simulation:** For each case in the DoE, this step performs the major disciplinary analysis to size the vehicle, including estimation of aerodynamic characteristics, vehicle weight build-up, propulsion system characteristics, mission analysis, and point performance evaluation, etc.
5) **Design space exploration:** With the simulated results of the sampling cases, a surrogate model is constructed for each response variable using multivariate regression technique. These surrogate models are then used to study the contributions of design variables to variation in metrics of interest, perform Monte Carlo simulations to investigate design feasibility within the design space, and optimize the design based on desirability.
6) **Uncertainty analysis:** The uncertainties include the epistemic uncertainties from disciplinary analyses and the technological uncertainties from novel technologies implementation. A DoE on the uncertainty variables is conducted and the resulting surrogate model is used to identify the impact of uncertainty variables on HWB sizing and optimization.

III. Disciplinary Analyses

A. Aerodynamics

Traditionally, the aerodynamic characteristics of tube-and-wing aircraft can be estimated using semi-empirical drag build-up methods, as is done in FLOPS [22], etc. However, due to the lack of flight testing and experimental data, such methods can be less accurate or biased for unconventional configurations including the HWB. Specifically, the FLOPS drag build-up method is known to over-predict the drag of HWB [4] which leads to higher estimated fuel consumption and therefore a higher vehicle gross weight. Due to the importance of accurate aerodynamic prediction in conceptual design, physics-based methods should be employed.

The selection of physics-based aerodynamic analysis method is a trade-off between accuracy and computational cost. Although high-fidelity methods such as the Navier–Stokes computational fluid dynamics (CFD) and the Euler CFD are theoretically more accurate compared with other simplified methods, they are computationally too expensive to be integrated in a conceptual sizing environment for design space exploration where a large amount of design candidates

are evaluated. On the other hand, low-fidelity methods such as the vortex lattice method are based on linearized theories, allowing for very quick estimation of aerodynamic characteristics, but at a cost of relatively low accuracy due to their inability to capture shocks in transonic flight conditions. Medium-fidelity methods such as the full velocity potential equations or the transonic small disturbance method are still time-consuming in 3-D analysis, let alone they are not capable of predicting strong shocks and flow separation behind the shock in transonic regime where commercial jetliners spend the most time in a mission. Therefore, the aerodynamic analysis employed in this work shall balance accuracy and execution time.

This paper proposes a multi-fidelity approach, a combination of 2-D Navier–Stokes CFD, 3-D vortex lattice method, and surrogate modeling. The 2-D Navier–Stokes CFD has the capability of capturing shocks (if any) and viscous drag of high fidelity. The 3-D vortex lattice method is used to compute the induced drag with compressibility correction as well as the parasite drag in conjunction with the 2-D CFD results. Surrogate models are created to substitute the 2-D CFD analysis in the aircraft sizing loop in order to reduce execution time and avoid potential convergence issues. The following subsections discuss each aspect in more detail.

1. Two-Dimensional Analysis

The 2-D CFD analysis is not a part of the aircraft sizing loop. Instead, it is conducted to generate lift and drag data of a series of airfoils at different flow conditions prior to vehicle sizing. These data are used to create surrogate models, which are later imported in the sizing loop to provide necessary information for the 3-D aerodynamic analysis. It is assumed that the outboard wing uses NASA-SC series supercritical airfoils [23] with design lift coefficients of 0.4, the vertical tails use symmetric NASA-SC supercritical airfoil, and the centerbody uses the LW109A reflexed airfoil [2]. The outboard wing airfoils are characterized by their thickness-to-chord ratios, z_t. The flow condition is characterized by the angle of attack, α, the Mach number, M, and the Reynolds number, Re.

Each CFD simulation takes a combination of M, Re, z_t, and α as the inputs, and computes the 2-D lift coefficient, C_l, and drag coefficient, C_d. The ranges of non-dimensional flow condition parameters (M, Re, and α) are determined such that the sample space covers a normal flight envelope throughout a mission. The simulations are performed in StarCCM+ [24] using the Reynolds-averaged Navier–Stokes solver (K-Omega turbulence model) and a solution-based adaptive mesh.

For compatibility with the 3-D aerodynamic analysis tool (Sec. III.A.2), the airfoil drag polar at given Mach number and Reynolds number is approximated using the quadratic polynomial in Eq. (1):

$$C_d \approx C_{d0} + K_1 C_l^2 + K_2 C_l \tag{1}$$

where the zero-lift drag coefficient, C_{d0}, and coefficients K_1 and K_2 are computed based on sample C_l and C_d values at given Mach number and Reynolds number. Such process is repeated for all combinations of M, Re, and z_t to create a surrogate model which predicts C_{d0}, K_1, and K_2 as shown in Eq. (2):

$$(\hat{C}_{d_0}, \hat{K}_1, \hat{K}_2) = \hat{f}\,(M, Re, z_t) \tag{2}$$

When Eq. (2) is used to estimate the parameters, M takes the local normal Mach number calculated based on freestream Mach number and local leading edge sweep; Re is calculated based on freestream condition and local chord length; z_t is the local airfoil thickness-to-chord ratio. As such, the sectional drag coefficient at given C_l can therefore be estimated using Eq. (3):

$$\hat{C}_d = \hat{C}_{d_0} + \hat{K}_1 C_l^2 + \hat{K}_2 C_l \tag{3}$$

2. Three-Dimensional Analysis

The 3-D aircraft aerodynamic analysis is conducted using Athena Vortex Lattice (AVL), a publicly available vortex lattice method solver [25]. In the aircraft sizing loop, AVL is used to compute the aircraft drag coefficients at certain freestream Mach number, altitude, and aircraft lift coefficient, which are then arranged into look-up tables compatible with FLOPS. The 2-D drag polar parameters ($\hat{C}_{d0}$, $\hat{K}_1$, and $\hat{K}_2$) are computed using Eq. (2) at the centerline, each wing station, and the root and tip of the vertical tails, respectively. Internally, AVL computes the induced drag and the profile drag which add up to the overall drag of the aircraft. The induced drag is computed using the vortex lattice method and corrected based on Göthert's rule for given aircraft geometry, overall lift coefficient, and Mach number. To account for non-isentropic and viscous effects which the vortex lattice method is unable to capture, the profile drag is computed based on the aircraft geometry and the 2-D drag polar parameters.

Results from 3-D analysis are ultimately used to generate aircraft-level aerodynamic data for FLOPS mission analysis. The customized aerodynamic data in FLOPS input file are characterized by two surrogate models and are entered as look-up tables:

$$C_{DO} = \hat{g}_1 (h, M) \tag{4}$$

$$C_{DI} = \hat{g}_2 (M, C_L) \tag{5}$$

where C_{DI} is the lift-dependent drag coefficient, and C_{DO} is the lift-independent drag coefficient [26]. The overall drag coefficient, C_D, corresponding to given altitude, Mach number, and aircraft lift coefficient is computed as

$$C_D (h, M, C_L) = C_{DO} (h, M) + C_{DI} (M, C_L) \tag{6}$$

3. Benchmarking

To validate the quality of the aerodynamic analysis method, a benchmark study was conducted by comparing the analysis result against experimental data. However, due to the lack of literature in public domain which documents experimental values of C_L and C_D for HWB, only three data points from the Boeing BWB-0009A model [20, 27] can be used for comparison. Using the the planform of Boeing BWB-0009A, a simplified benchmark HWB model as shown in Fig. 1 was established and evaluated through the aerodynamic analysis environment. The results are compared with known data [20, 27] as shown in Table 2. It is believed that the accuracy of proposed multi-fidelity approach is sufficient to serve the purpose of this work. The errors in prediction of aerodynamic characteristics will be addressed in uncertainty analysis (Sec. VI).

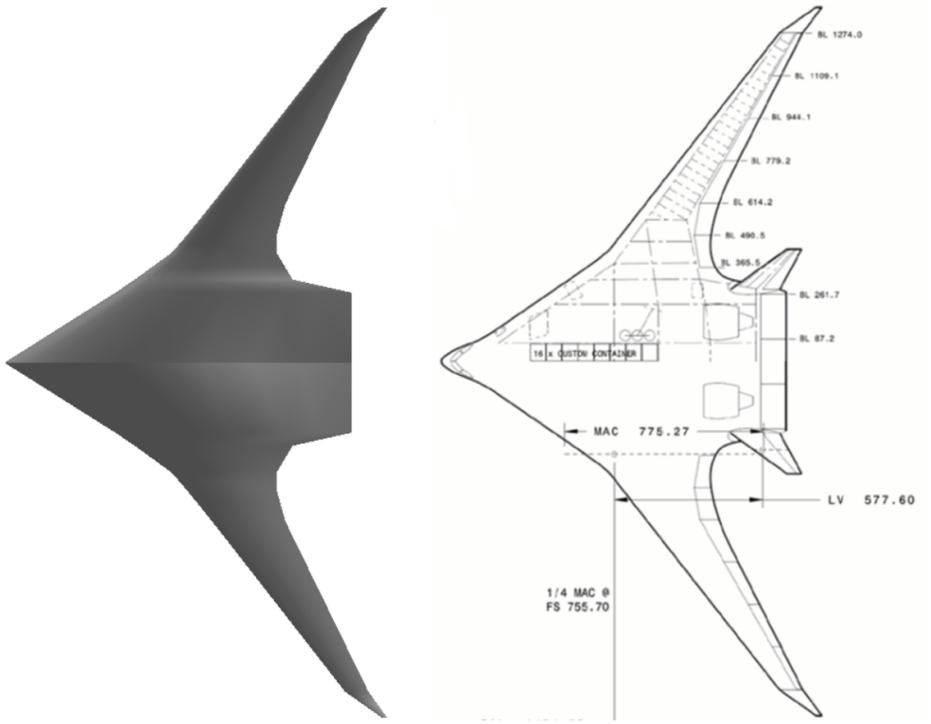

Fig. 1 Geometry comparison between benchmark model and BWB-0009A[20]

B. Weight Estimation

An accurate estimation of the empty weight is critical in aircraft design process. Existing tools using physics-based methods include RADE which focuses on structural sizing and weight estimation of the airframe and lifting surfaces [28], ISSAAC which sizes major aircraft subsystems [29], and WATE++ which analytically computes engine weight and dimension [30], etc. However, to achieve a high fidelity, physics-based methods typically require a large amount of

Table 2 Comparison of lift-to-drag ratio between experimental data and proposed approach

Flight condition	Boeing report [20, 27]	Proposed approach	% Error
$M = 0.85, h = 35000$ ft, $C_L = 0.2412$	23.92	23.02	−3.78
$M = 0.85, h = 39000$ ft, $C_L = 0.2067$	22.64	22.83	0.88
$M = 0.85, h = 43000$ ft, $C_L = 0.2119$	22.38	22.72	1.52

inputs, part of which are beyond the design knowledge in the conceptual level. Also, as the fidelity of analysis increases, especially with high-resolution finite element models, the computational cost and execution time can become prohibitive for an efficient design space exploration at the conceptual level.

Meanwhile, there also exist semi-empirical regression-based methods such as Roskam [31], Raymer [17], and FLOPS [32]. The FLOPS method is employed in this paper since it has been modified to account for the special HWB geometry and has developed a new set of equations, enabling the weight estimation for HWB fuselage and aft body [32]. In general, the FLOPS method provides a fast weight estimation for major aircraft elements including structural components, propulsion system, and subsystems and equipment.Compared to physics-based methods, FLOPS mainly uses top-level geometric parameters, design mission specification, and operating limits to perform the estimation, most of which are known or controllable by the designer in the conceptual design phase.

C. Propulsion System

Due to lack of knowledge at the conceptual design phase and excessive runtime required by related software, a detailed engine cycle analysis is not carried out for each design candidate analyzed in this work. Instead, a baseline engine deck is generated once along with the sizing of the baseline aircraft, using the Numerical Propulsion System Simulation software (NPSS) [33] for engine cycle analysis and WATE++ [30] for estimation of engine weight and dimension. The baseline engine is assumed to be a 2005 technology level geared turbofan [27]. In the subsequent design space exploration, the engine deck is scaled up or down depending on the thrust required. The dimension, weight and fuel flow of the engine are also scaled accordingly [32].

All design candidates are assumed to carry fuel in the outboard wing section. This work adopts the FLOPS method [32] to estimate fuel tank volume and redefines several parameters to be compatible with HWB geometry:

$$V_{tank} = k z_t \frac{S_w^2}{b}\left(1 - \frac{\lambda}{(1+\lambda)^2}\right) \tag{7}$$

where V_{tank} is the total volume of fuel tanks, k is a non-dimensional volume coefficient, b is redefined as the total span of the portion of the wing that is equipped with fuel tanks, and λ is the taper ratio of the wing section equipped with fuel tanks. In this work, the fuel tank volume coefficient k is set to 3.9 which is estimated from data of existing tube-and-wing LTA models [27].

IV. Design Variables and Baseline Aircraft

A. Design Variables

Conventionally, in conceptual design of tube-and-wing aircraft, there is little interaction between the planform geometry of fuselage and wing, which can therefore be sized independently. For HWB, the special geometry joining the fuselage and wing results in additional geometric constraints. Specifically, the airfoils at the side of centerbody and at the outboard wing root must match each other in terms of shape and dimension. This section clarifies the definition of design variables used in this paper and briefly discusses how the wing-fuselage geometric coupling effects are addressed.

1. Centerbody Fuselage

This paper uses the FLOPS method for HWB cabin sizing and layout [4, 32]. The parameters used to determine fuselage size and shape include passenger capacity of each cabin class, length of cabin side wall (XLW), sweep angle of the centerbody leading edge (SWPLE), and chordwise locations of rear spar at centerline (RSPCHD) and side of fuselage (RSPSOB). The number of passengers, which is a requirement from request for proposal and remains invariant

for all design candidates, is used to determined the total cabin area required. The other variables are used to determine the detailed planform geometry of the centerbody. In this paper, RSPCHD and RSPSOB are fixed at the default value of 70% of local chord length. XLW and SWPLE remain the two design variables being varied in designs space exploration.

2. Outboard Wing

In conceptual design of conventional tube-and-wing aircraft, the wing planform geometry can be treated as a trapezoid independent of fuselage geometry and can be parametrically defined using five variables: aspect ratio (AR), taper ratio (TR), average thickness-to-chord ratio (TCA), quarter-chord sweep angle (SWEEP), and wing area (SW). Among them, AR, TR, TCA, and SWEEP are non-dimensional scaling parameters, while SW is usually dynamically computed based on wing loading (WSR) during sizing iterations. However, due to the additional wing-centerbody geometric constraint for HWB, variables in this set are not independent of each other. This constraint makes AR, TR, and SW correlated once the length of centerbody outboard wall is determined, reducing one degree-of-freedom in selecting free design variables. The FLOPS method proposes two solutions for outboard wing definition [26]:

1) Explicitly specify the dimensional tip chord length (TIPCHD). The wing tip is then simply connected to the fuselage side wall to form a trapezoidal wing planform based on a given span or wing area. This method is considered too restrictive to represent a real HWB wing on which the variation of wing chord length with respect to spanwise location is typically nonlinear (or piecewise linear).
2) Explicitly specify the outboard semispan (OSSPAN). This solution requires a detailed wing definition where the spanwise location (ETAW), chord length (CHD), and thickness (TOC) at each wing station are well-defined. Meanwhile, the sizing parameters used in conventional aircraft, such as AR, TR, TCA, and SW, are incompatible in this mode. Making ETAW, CHD, and TOC at each station independent will result in too many design variables, which drastically increases the computational cost for design space exploration.

While this work still adopts the high-level scaling parameters AR, TR, TCA, and SWEEP, for compatibility with HWB configuration, AR and TR are redefined as follows:

$$AR = \frac{4 \times OSSPAN^2}{SW} \tag{8}$$

$$TR = \frac{CHD_n}{XLW/RSPSOB} \tag{9}$$

where n is the number of wing stations and CHD_n is the length of tip chord. For compatibility with FLOPS settings, OSSPAN is activated, and an external wrapper is made to convert the redefined high-level geometric design variables to detailed wing geometric parameters (ETAW, CHD, and TOC) with following rules:

1) The normalized spanwise locations of wing stations (ETAW, fraction of outboard wing semispan) are held constant for each design candidate in the sizing loop.
2) The length of wing root matches the length of fuselage side wall.
3) Except for wing root, the chord length (CHD) at each wing station is calculated based on root chord, TR and ETAW such that the geometric similarity is maintained.
4) The thickness-to-chord ratio (TOC) at each wing station is scaled proportionally to TCA.

In this work, the wing is regarded as multiple trapezoidal sections, therefore SW, OSSPAN, CHD, and ETAW are related through the following equation:

$$SW = OSSPAN \times \sum_{i=1}^{n-1} [(CHD_i + CHD_{i+1}) \times (ETAW_{i+1} - ETAW_i)] \tag{10}$$

Given the fuselage geometry and TR, ETAW and CHD are fisrt determined following the four rules above. SW and OSSPAN can then be derived from AR through Eqs. (8) and (10).

3. Empennage

The design variables of vertical tail and horizontal tail include aspect ratios (ARVT and ARHT), taper ratios (TRVT and TRHT), and quarter-chord sweep angles (SWPVT and SWPHT). The areas of vertical tail (SVT) and horizontal tail

(SHT) are calculated using Eqs. (11) and (12):

$$VTVC = \frac{XL \times SVT}{SW \times \sqrt{SW \times AR}} \tag{11}$$

$$HTVC = \frac{XL \times SHT}{SW \times \sqrt{SW/AR}} \tag{12}$$

where XL is the length of fuselage centerline. VTVC and HTVC are the modified tail volume coefficients [32] which are determined from the baseline geometry and held constant for all design candidates. Since the baseline configuration (Sec. IV.B) is not equipped with a horizontal tail, this paper considers exclusively the vertical tails.

4. Aircraft-level Sizing Parameters

In traditional aircraft sizing process, the thrust-to-weight ratio (TWR) and the wing loading (WSR) are often regarded as the top-level sizing parameters [18]. The wing area is then dynamically computed from wing loading and design gross weight at each sizing iteration. However, for HWB configuration, since AR, TR, and SW are correlated due to the wing-fuselage geometric constraint, if AR and TR are chosen as design variables independent of fuselage geometry, then SW (and subsequently WSR) will be a fall-out. Such decision eliminates WSR from the choices of design variables. Note that this process can be amended such that WSR becomes an independent design variable, in which case either AR or TR needs to be deactivated. Per discussions above, in this paper, the only active independent top-level sizing parameter is TWR, defined as

$$TWR = \frac{NENG \times THRUST}{DGW} \tag{13}$$

where NENG is the number of engines (in this work NENG = 2 for a twin-jet) and THRUST is the required rated thrust per engine.

B. Baseline Aircraft

As a proof of concept for the sizing and optimization framework, the ASDL 300-pax HWB LTA RTC model [27] is selected as the baseline aircraft. Figure 2 shows the baseline aircraft geometry and the AVL model used for aerodynamic analysis. A generic mission profile for commercial transport is assumed for the design mission. Table 3 presents key geometry and performance specifications of the baseline aircraft.

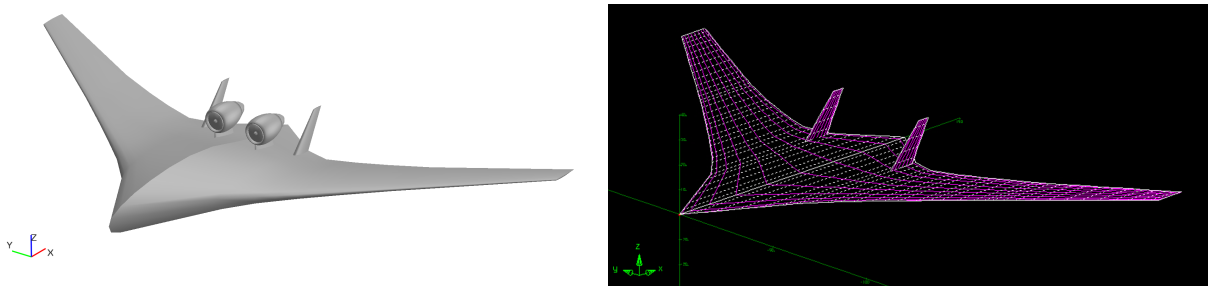

Fig. 2 VSP and AVL models of baseline aircraft

V. Design Space Exploration

The design space of interest is constructed using the design variables defined in Section IV.A and their associated ranges, as shown in Table 4. The design space exploration follows the steps developed by Kirby et al. [34], which include design of experiments, surrogate modeling, sensitivity studies on design variables, feasibility evaluation, and multi-objective optimization. The statistical analysis tool JMP is used for the practice of design space exploration.

Table 3 Baseline aircraft specifications

Parameter	Value	Unit
Passenger capacity	305	-
Maximum ramp weight	509 272	lb
Design range	7530	nmi
Cruise Mach number	0.84	-
Sea-level static thrust	$2 \times 33\,976$	lb
Outboard wing aspect ratio (AR)	6.84	-
Outboard wing taper ratio (TR)	0.196	-
Outboard wing 1/4-chord sweep (SWEEP)	36.0	deg
Outboard wing thickness-to-chord (TCA)	0.110	-
Outboard wing semi-span	104.8	ft
Planform area	10 646	ft^2
Cabin side wall length (XLW)	45.0	ft
Fuselage leading edge sweep edge (SWPLE)	60.0	deg
Cabin centerline length	84.6	ft
Cabin width	45.7	ft
Cabin area	2961	ft^2
Chordwise location of rear spar	0.70	-
Total fuselage length	121	ft
Maximum fuselage depth	20.0	ft
Vertical tail aspect ratio (ARVT)	1.95	-
Vertical tail taper ratio (TRVT)	0.464	-
Vertical tail 1/4-chord sweep (SWPVT)	39.4	deg
Vertical tail planform area	140	ft^2

Table 4 Ranges of design variables

Design variables	Low	High	Unit
Thrust to weight (TWR)	0.2	0.35	-
Outboard wing aspect ratio (AR)	5.47	8.21	-
Outboard wing taper ratio (TR)	0.16	0.23	-
Outboard wing 1/4-chord sweep (SWEEP)	28.80	43.20	deg
Outboard wing thickness-to-chord (TCA)	0.09	0.13	-
Cabin side wall length (XLW)	38.27	51.77	-
Fuselage leading edge sweep angle (SWPLE)	48.00	72.00	deg
Vertical tail aspect ratio (ARVT)	1.56	2.34	-
Vertical tail taper ratio (TRVT)	0.37	0.56	-
Vertical tail 1/4-chord sweep (SWPVT)	31.54	47.30	deg

A. Surrogate Modeling for Design Variables

Designs of experiments (DoEs) are performed to sample the design space in a structured manner, from which a surrogate model is constructed for the metrics of interest. The use of surrogate model then enables fast evaluation of design candidates within the design space without calling the true analysis.

The evaluation of a design candidate involves predicting its drag polar using AVL and surrogate models of 2-D drag

polar coefficients, and evaluating vehicle-level metrics using FLOPS. On a quad-core desktop personal computer, each drag polar takes approximately 12 min of CPU time to generate from a series of AVL executions, while given an aircraft drag polar, each vehicle takes approximately 0.5 sec of CPU time to evaluate in FLOPS.

The DoE for the design variables includes 149 samples from a face-centered central composite design (CCD) and 200 samples from a Latin-hypercube design. The surrogate model for has the following general form:

$$\log y \approx P_{3,DV}(TWR, AR, ..., SWPVT) \tag{14}$$

where y is a response variable, and $P_{3,DV}(\cdot)$ is a third-order polynomial for the design variables whose coefficients are determined using multivariate linear regression. 200 additional cases are generated randomly in design space to validate the surrogate model through the model representation error (MRE), i.e. the error between true function value and predicted value. The distribution of the MRE for metrics of interest of the 200 validation cases is shown in Fig 3. Since the MRE can be approximated using a normal distribution with mean about 0 and standard deviation less than 1%, the surrogate model is considered valid to represent the true analysis in design space.

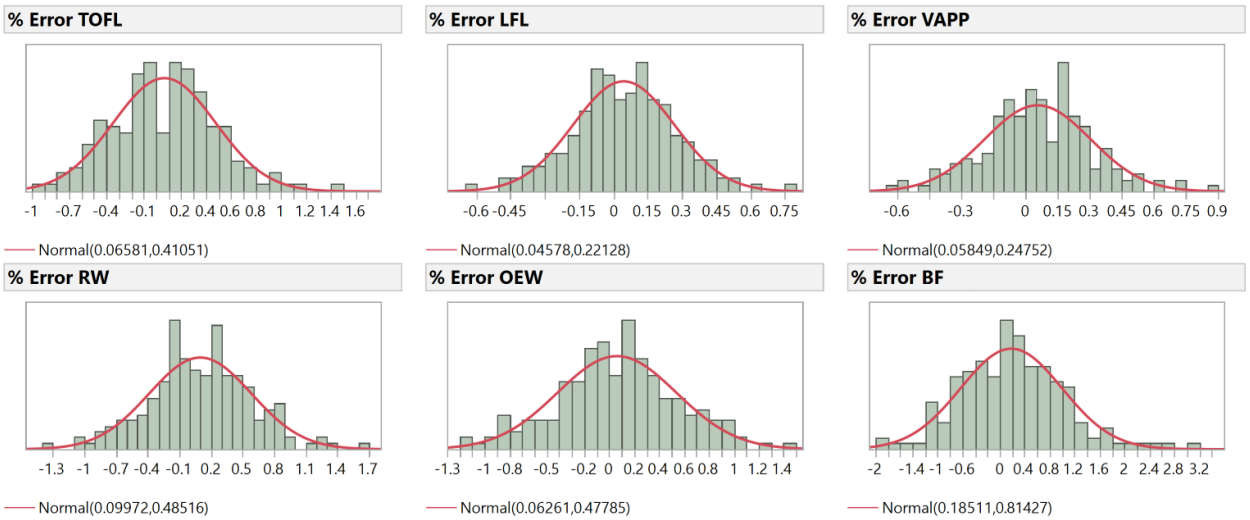

Fig. 3 MRE distributions for design variables surrogate model

B. Sensitivity Analysis

The sensitivity analysis performed in this section investigates the responses of vehicle-level metrics with respect to variation in design variables. A prediction profiler plot generated from the surrogate model in Eq. (14) is shown in Fig. 4, where the design variables are plotted on the horizontal axes and the metrics on the vertical axes. The horizontal axis intervals are set based on Table 4, and the vertical axis intervals are set to ±10% of the current value indicated by the crosshair. The impact of each design variable on the metrics of interest are indicated by the local slope of prediction traces and the height of triangles, which indicate the magnitude of partial derivative evaluated at the current design variable settings.

Based on Fig. 4, the impacts of top-level vehicle sizing parameter and wing-body planform variables are much significant than the vertical tail variables. The sizing parameter TWR has the most significant impact on takeoff field length. Among planform variables, AR has the most significant impact on aircraft weight since the wing structural weight increases with AR due to increased wing bending moment; on the other hand, higher AR values also significantly improve takeoff and landing performance due to the improvement in aerodynamics characteristics. TR affects the metrics of interest in a similar manner as AR does on weights and fuel burn, but the effect is less significant on takeoff and landing performance. The sweep angles of outboard wing (SWEEP) and fuselage (SWPLE) have the most significant impact on block fuel through high-speed aerodynamic characteristics during cruise. Their impact on structural weight is subtle at small values, but becomes significant at large values. As a consequence, at large sweep angles, the rapidly increasing structural weight negates the aerodynamic benefits, causing an increase in ramp weight and diminishing improvements in takeoff and landing performance.

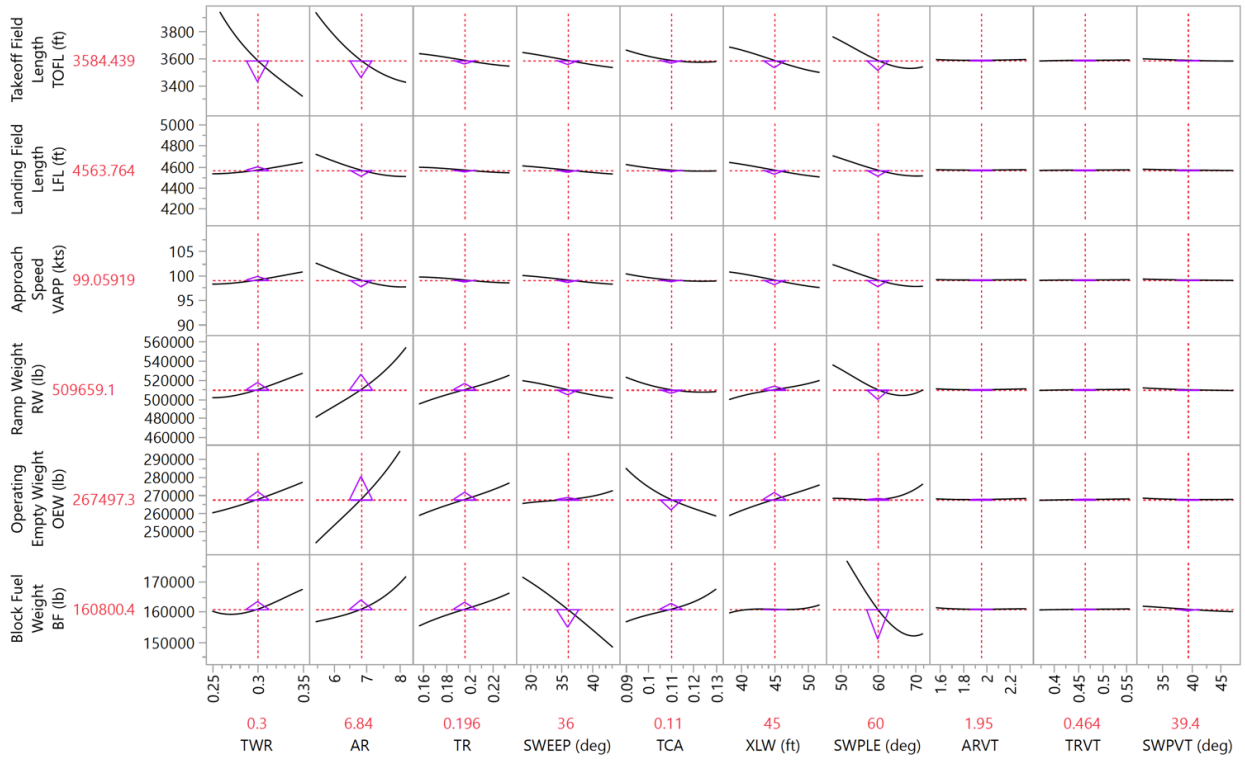

Fig. 4 Impact of design variables on metrics of interest

C. Feasibility Evaluation

The feasibility evaluation assesses the feasible design space confined by design constraints. The constraints can arise from multiple sources such as customer requirements, regulations, and operations, etc. In this work, three types of constraints are considered:

Table 5 N+2 performance constraints

Performance Metric	"N+2" Goal	Reference Value	HWB Constraint
Block Fuel	−40%	249 180 lbs [27]	≤ 149 508 lbs
Takeoff Field Length	−50%	11 050 ft [35]	≤ 5525 ft
Landing Field Length	−50%	5250 ft [35]	≤ 2625 ft

Table 6 FAA Airplane Design Group [36]

Group	Wingspan (ft)	Typical Aircraft
V	171− < 214	B777, B787, A330
VI	214− < 262	B747-8, A380

1) *Performance constraints*. These include the "N+2" requirements on fuel burn and field length improvements as mentioned in Table 1. The target constraint values shown in Table 5 are computed by applying the goal of improvement on the performance data of a representative 300-passenger LTA tube-and-wing model [27, 35].
2) *Physical constraints*. The vehicle must be physically capable of operating the design mission. This work considers the fuel constraint dictated by the excess fuel capacity for the design mission, which is computed as the difference between the loaded fuel and the maximum fuel capacity. The excess fuel capacity must be non-negative for design feasibility.

Table 7 FAA Airplane Approach Category [36]

Category	Approach Speed	Typical Aircraft
A	Less than 91 knots	DHC-7, Beech 55
B	91 knots or more but less than 121 knots	ATR-42, Dash 8
C	121 knots or more but less than 141 knots	B737-700, CRJ900

3) *Operational constraints*. These include the major constraints imposed by existing airport facilities that have been constructed based on a series of aircraft categories. The constraint values are presented in Tables 6 and 7 based on FAA Airport Design Advisory Circular [36].

To explore the design space and examine feasibility, a Monte Carlo simulation is performed on the design variable surrogate model (Eq. (14)). The Monte Carlo simulation is a probabilistic technique which randomly generates values for design variables based on the assigned probability distribution [34]. In this work, 100 000 designs are randomly generated where each design variable is drawn from a uniform distribution within the intervals in Table 4. These cases are then rapidly simulated using the surrogate model.

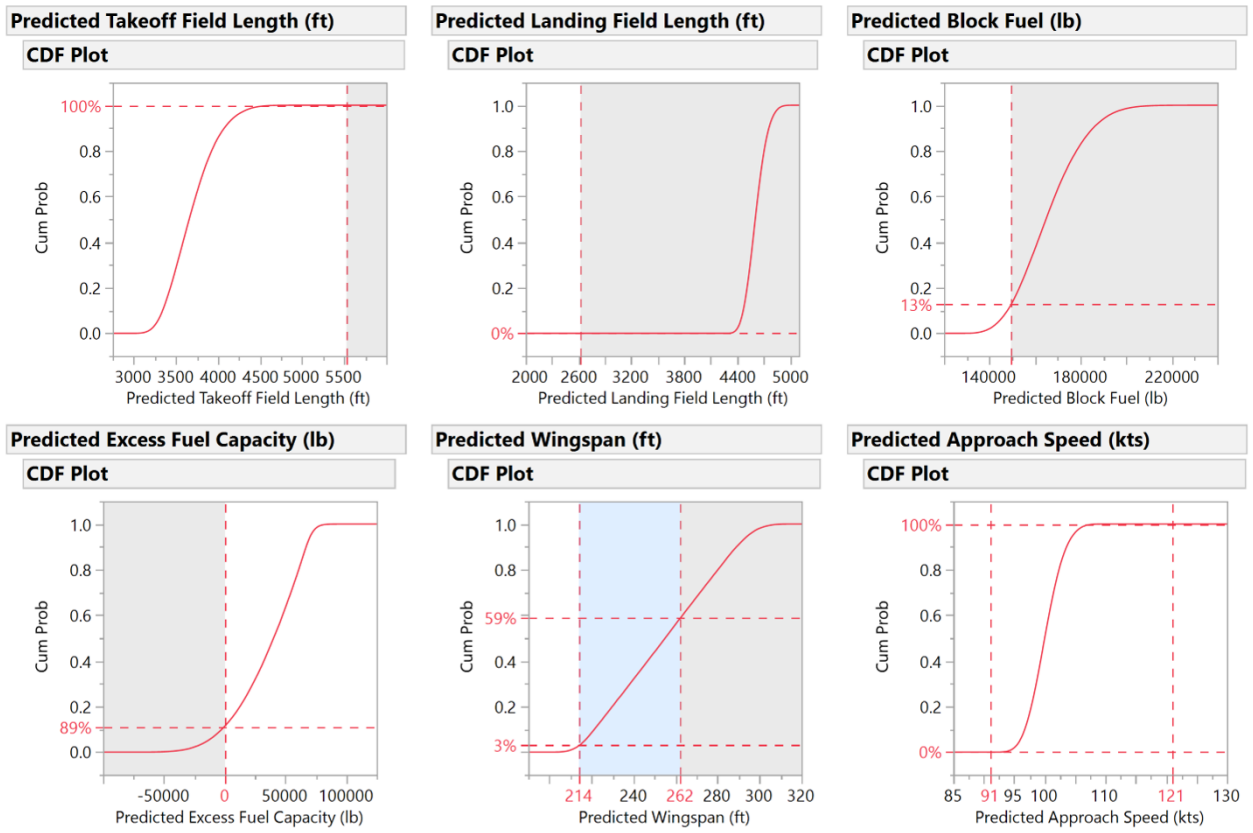

Fig. 5 CDF plots for feasibility assessment

The feasibility is assessed by first inspecting the Cumulative Distribution Functions (CDF) plot of each constraint variable shown in Fig. 5. The threshold values are marked on the horizontal axis, and the infeasible intervals are grayed out. The label of the crosshair on the vertical axis indicates the rate of success, i.e. the probability that a design randomly selected in the design space is feasible when the corresponding constraint is considered individually. A rate of success of 100% (e.g. takeoff field length) implies that the constraint is inactive within the entire design space, while a rate of success of 0% (e.g. landing field length) indicates that the constraint is a show-stopper for the design space which must be relaxed in order to obtain a feasible design. Since the takeoff field length constraint is never active, and the landing field length requirement has been considered challenging for HWB as discussed in literature [20], they are

both deactivated in the following discussion. It can also be observed that all simulated cases satisfy the FAA Airplane Approach Category B requirement on approach speed, which includes mostly regional turboprop aircraft. Constraints which show a rate of success between 0 and 1 need further study in order to examine the design space feasibility when these constraints are considered simultaneously.

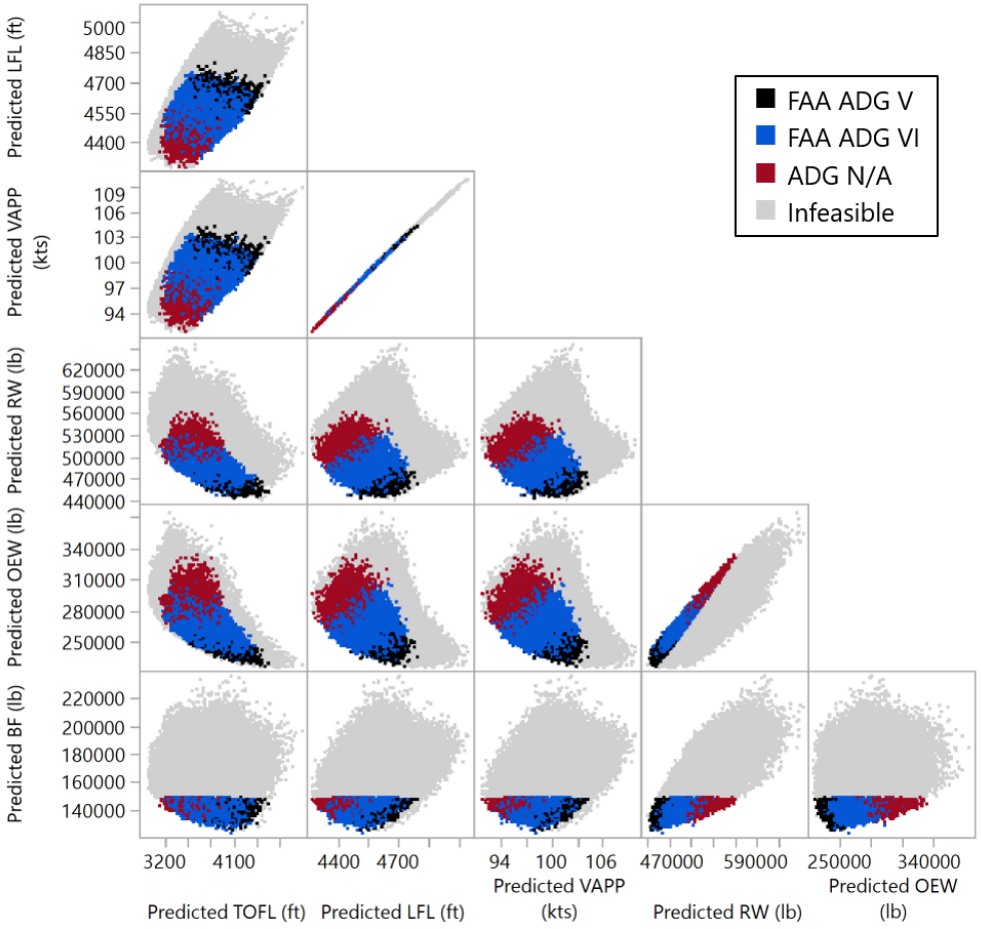

Fig. 6 Filtered scatterplot matrix for feasibility assessment

Figure 6 presents a scatterplot matrix for the metrics of interest generated using JMP. Each subplot shows a projection of the design space onto a bivariate plane. The feasible design space can be identified by applying filters based on constraints. The excess fuel capacity constraint and the block fuel reduction constraint are first applied to rule out the infeasible design space. The wingspan constraint is then applied sequentially at two threshold values based on the FAA Aircraft Design Group (ADG) in Table 6. Designs which violate the maximum wingspan constraint of Group VI are not instantly considered infeasible at this stage, since novel technologies may be infused to morph the wing during ground operations, e.g. folding wing, whose risk assessment and impact on weight estimation are beyond the scope of this work. Note that a more restrictive wingspan constraint has a negative impact on the takeoff and landing performance, but at the same time also permits the vehicle to operate at more existing airport whose facilities have been built according to the ADG requirements.

Figure 7 plots the metrics and constraints against all design variables for the simulated cases, with the same constraint filter applied. When considering the performance and physical constraints, lower sweep angles (SWPLE and SWEEP) are less likely to yield a feasible design. Enforcing wingspan constraint leads to a decrease in maximum permissible value of AR.

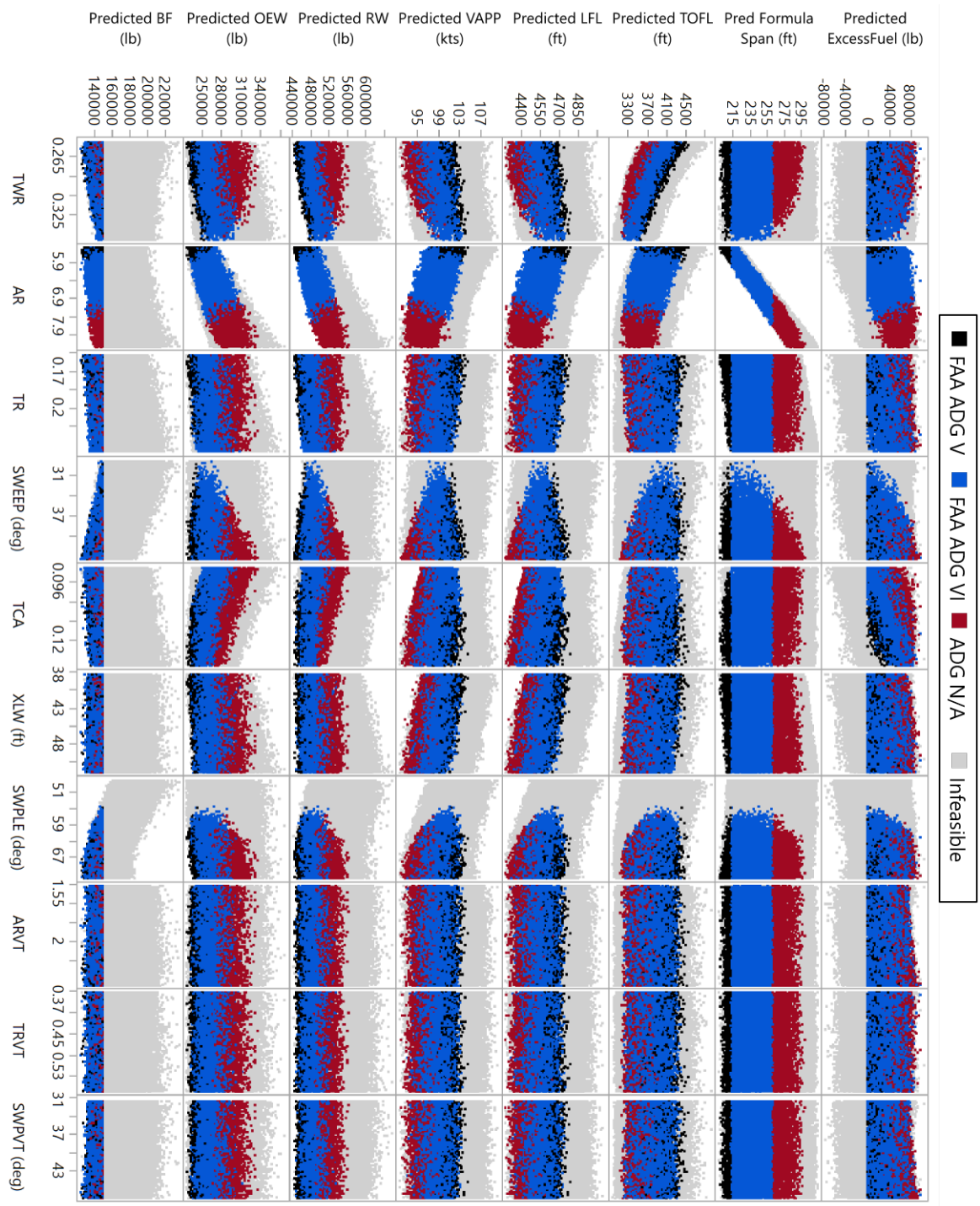

Fig. 7 Filtered scatterplot matrix for feasibility assessment

D. Multi-objective Optimization

A constrained multi-objective optimization is conducted in the design space using the desirability function facilitated in JMP. The desirabilities of performance metrics (TOFL, LFL, VAPP, BF, RW, and OEW) are set as minimization, and each metric is assigned equal importance of desirability. The optimization is subject to the excess fuel constraint and FAA ADG VI wingspan constraint. The surrogate model in Eq. 14 is used as the objective function. By maximizing the

desirabilities, an optimized design is obtained within the design space. The set of design variables that maximize the desirability function are listed in Table 8. The geometry comparison between the baseline and the optimized design is presented in Table 8 and Fig. 8.

Table 8 Comparison of baseline and optimized design

Design Variable & Metric	Baseline Design	Optimized Design	Improvement
Thrust to weight (TWR)	0.3	0.27	-
Aspect ratio (AR)	6.84	6.89	-
Taper ratio (TR)	0.196	0.157	-
1/4-chord sweep (SWEEP)	36.0	43.2	-
Thickness to chord (TCA)	0.110	0.130	-
Cabin side wall length (XLW)	45.0	51.8	-
Fuselage leading edge sweep (SWPLE)	60.0	69.1	-
Vertical tail aspect ratio (ARVT)	1.95	1.62	-
Vertical tail taper ratio (TRVT)	0.464	0.556	-
Vertical tail 1/4-chord sweep (SWPVT)	39.4	31.8	-
Takeoff field length (TOFL)	3585	3529	1.56%
Landing field length (LFL)	4563	4353	4.60%
Approach speed (VAPP)	99.0	93.9	5.15%
Ramp weight (RW)	509 272	470 478	7.62%
Operating empty weight (OEW)	267 607	255 854	4.39%
Block fuel (BF)	160 282	136 754	14.7%

VI. Uncertainty Analysis

The uncertainty analysis investigates the impact of uncertainties on sizing and optimization results. Two types of uncertainties are considered. Epistemic uncertainties arise from the assumptions and modeling errors of disciplinary analyses, such as the error in drag prediction and weight estimation, etc. Technological uncertainties are due to the implementation of new technologies, such as technologies which reduce drag, fuel burn, and structural weight, as well as new subsystem architectures, etc. which might be realized on future aircraft, but since their Technology Readiness Levels (TRLs) are still low as of now, it is difficult to precisely capture their effects in current sizing process.

The effects of epistemic and technological uncertainties are modeled by "K-factors" which are a set of multiplicative factors applied to intermediate results of disciplinary analyses including aerodynamics, propulsion, and weight estimation. Table 9 presents the eight uncertainty variables used in this paper and their ranges. The drag factor represents the uncertainties in aerodynamic prediction, the fuel flow factor represents the uncertainties in fuel consumption prediction in mission analysis, and the weight factors represent the uncertainties in weight predictions of aircraft components.

A. Surrogate Modeling for Uncertainty Factors

Naturally, due to compounding effects between vehicle weight, drag, and fuel burn in aircraft sizing, there exists interaction between the design variables and the K-factors. A combinatorial DoE where the ten design variables and eight K-factors are being varied simultaneously would be ideal to capture such interacting effects. However, given the available computational resources in hand, the authors were unable to perform such a large DoE where the large number of unique combinations of design variables would have required prohibitive AVL runtime at the stage of conceptual design.

It is hypothesized that the interaction between the design variables and the K-factors are negligible given their ranges in this paper. If the hypothesis is valid, the relative impact of K-factors on the metrics is independent of design variable settings. To test this hypothesis, a circumscribed CCD containing 81 samples is prepared exclusively for the K-factors to train a surrogate model, where all design variables are set to the center values in their ranges in Table 4. The surrogate

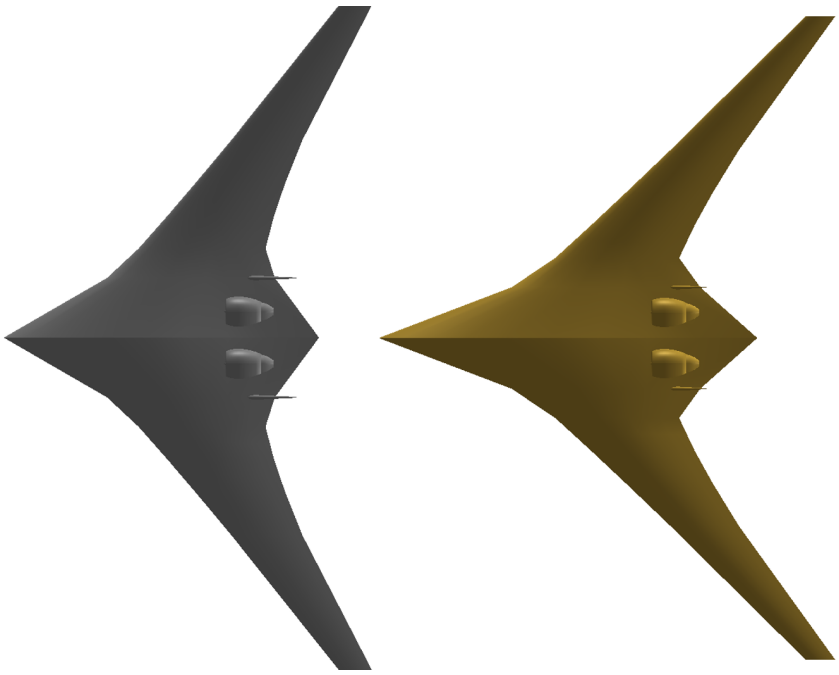

Fig. 8 Comparison of baseline (left) and optimized design (right)

Table 9 K-factors and sampling intervals

K-Factor	Low	Nominal	High
Factor for drag (FCDSUB)	0.9	1	1.1
Factor for engine fuel flow (FFFSUB)	0.9	1	1.1
Factor for wing weight (FRWI)	0.9	1	1.1
Factor for fuselage weight (FRFU)	0.9	1	1.1
Factor for vertical tail weight (FRVT)	0.9	1	1.1
Factor for engine weight (WENG)	0.9	1	1.1
Factor for landing gear weight (FRLG)	0.9	1	1.1
Factor for surface contorls weight (FRSC)	0.9	1	1.1

model for K-factors takes the following general form:

$$\log \frac{y}{y_0} \approx P_{2,K}(FCDSUB, FFFSUB, ..., FRSC) \tag{15}$$

where y_0 is the value of the response variable calculated with all K-factors set to 1, and $P_{2,K}(\cdot)$ is a second-order polynomial for the K-factors whose coefficients are determined using multivariate linear regression. Combined with Eq. (14), the complete surrogate model has the following form:

$$\hat{y} = \exp\left(P_3(TWR, AR, ..., SWPVT) + P_2(FCDSUB, FFFSUB, ..., FRSC)\right) \tag{16}$$

where $\hat{y}$ is the metric predicted value.

For model validation, the Cartesian product of a set of 200 random samples of design variables and a set of 50 random samples of K-factors (i.e. a total of 10 000 cases) are evaluated using both the design environment (AVL and FLOPS) and the combined surrogate model in Eq. (16). Note that the predicted aerodynamic characteristics is independent of K-factor settings. Therefore, the predicted aerodynamic characteristics from the 200 samples for testing evaluated in Sec. V.A can be reused, which significantly reduces computational cost in this step. Figure 9 shows the distributions of model representation error, all of which closely follow a normal distribution centered about 0 with

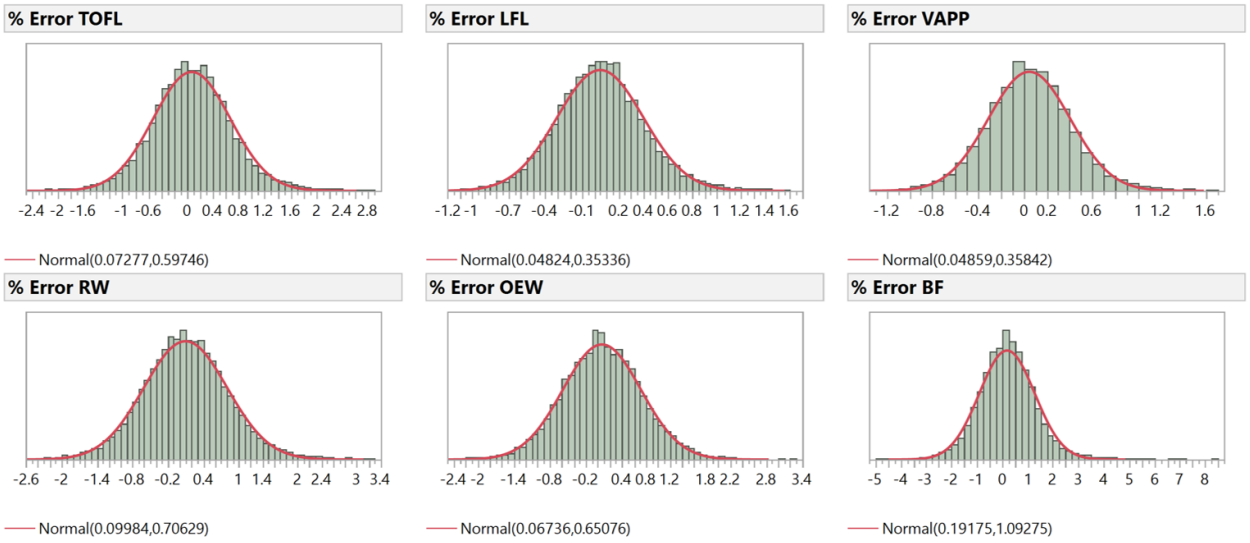

Fig. 9 MRE distributions for the combined surrogate model

standard errors less than 1.1%. Comparing the ranges of responses and the distribution of MRE, the hypothesis is considered valid. Subsequent discussion is therefore based on the surrogate model in Eq. (15).

B. Assessing Impact of Uncertainty

Figure 10 presents the prediction profilers for the K-factors generated using Eq. (15).For a fair comparison, the horizontal and vertical axis intervals are set equal in each subplot. Note that based on the discussions in Sec. VI.A, the interaction between the design variables and the K-factors is negligible, therefore the relative impact of K-factors on the responses is independent of design variable settings.

Among the K-factors considered, the uncertainties in drag and fuel flow prediction (FCDSUB and FFFSUB) contribute to the most variation in block fuel, and through compounding effects in aircraft sizing, cause significant variation in ramp weight, field lengths, and approach speed, but have a weaker effect on the operating empty weight. Since the wing and the fuselage are the largest structural elements of the vehicle, uncertainties in predicted wing weight and fuselage weight (FRWI and FRFU) have the most significant impact on OEW, which in turn affects ramp weight, takeoff field length, and block fuel. In comparison, since the weights of vertical tail, engines, landing gears, and surface control system account for only a small fraction of the empty weight, their uncertainties (FRVT, WENG, FRLG, and FRSC) have limited impact on the metrics.

VII. Conclusions

This paper presented an integrated sizing and optimization framework for the hybrid wing-body configuration by incorporating the physics-based disciplinary analyses with statistical methods. A multi-fidelity aerodynamic analysis approach combining 2-D CFD, vortex lattice method, and surrogate modeling is integrated as a module within the framework. The multi-fidelity approach is shown to be acceptable for HWB configuration aerodynamic prediction through a benchmark study with experimental data. The vehicle-level surrogate model enables efficient design space exploration, optimization, and uncertainty analysis. The sensitivity analysis performed on design variables shows that aspect ratio, centerbody leading edge sweep angle, and thrust-to-weight ratio contribute significantly to variation in performance metrics. The feasibility evaluation reveals that the HWB configuration is able to achieve the "N+2" performance improvement goals regarding fuel burn and takeoff field length while the landing field length requirement is a show-stopper. Better takeoff and landing performance can be achieved by relaxing the wingspan constraint which may cause issues in ground operation with existing airport facilities. Through uncertainty analysis, it is found that the errors in drag and fuel flow prediction has the most significant impact on fuel burn and, through compounding effects, vehicle weight and field performance. Avenues for future work include 1) incorporate other disciplines in sizing and optimization process, such as engine sizing, control surface sizing, subsystem sizing, etc; 2) use the framework

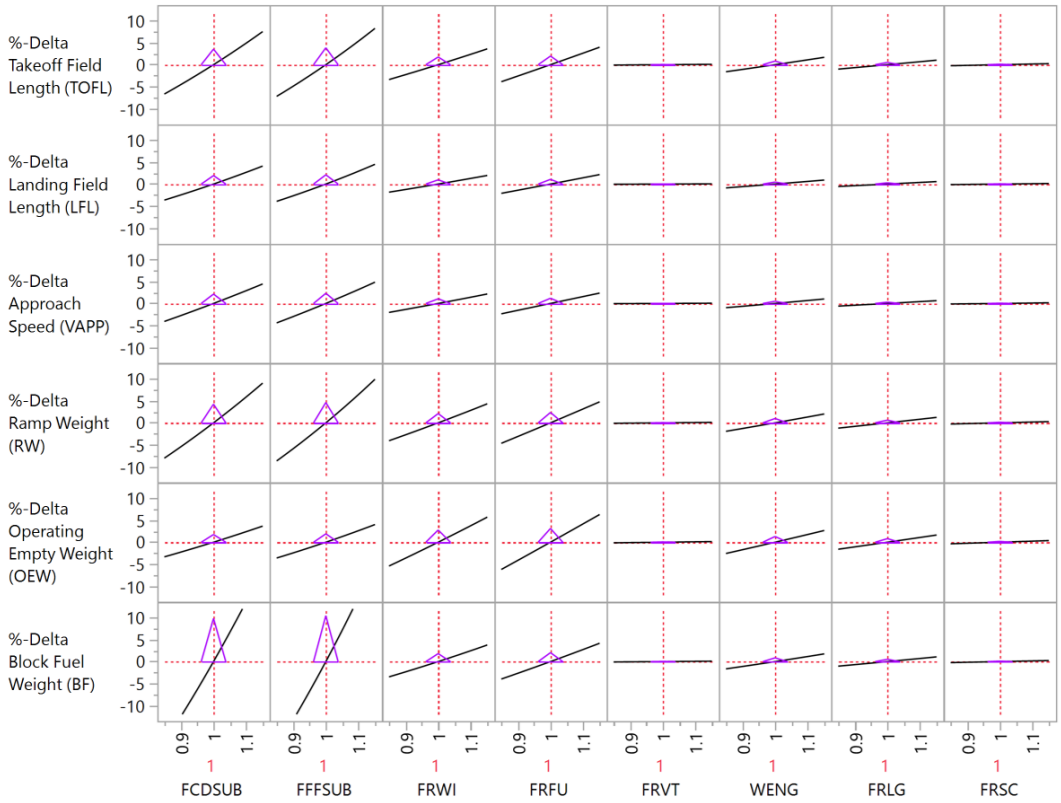

Fig. 10 Impact of uncertainty K-factors on metrics of interest

to analyze HWB designs of different size-classes, e.g. 100-pax regional aircraft and 500-pax very large aircraft, etc.; 3) identify a morphological matrix for all possible HWB configurations (e.g. tail configuration) and apply the framework to perform comparison across different configurations.

Acknowledgments

The authors would like to express their great appreciation to Professor Lakshmi Sankar for his valuable and constructive advising on the multi-fidelity aerodynamic analysis method proposed in this work.

References

[1] Mangelsdorf, M., "Environmentally Responsible Aviation N+2 Advanced Vehicle Concepts NRA Status," , Jun. 2011. URL `https://ntrs.nasa.gov/archive/nasa/casi.ntrs.nasa.gov/20110015351.pdf`.

[2] Liebeck, R. H., "Design of the Blended Wing Body Subsonic Transport," *Journal of Aircraft*, Vol. 41, No. 1, 2004, pp. 10–25. doi:10.2514/1.9084.

[3] Bradley, K. R., "A Sizing Methodology for the Conceptual Design of Blended-Wing-Body Transports," Tech. rep., George Washington University & NASA Langley Research Center, 2004.

[4] Nickol, C., and Mccullers, L., "Hybrid Wing Body Configuration System Studies," *47th AIAA Aerospace Sciences Meeting including The New Horizons Forum and Aerospace Exposition*, American Institute of Aeronautics and Astronautics (AIAA), 2009. doi:10.2514/6.2009-931.

[5] Brown, M., and Vos, R., "Conceptual Design and Evaluation of Blended-Wing Body Aircraft," *2018 AIAA Aerospace Sciences Meeting*, American Institute of Aeronautics and Astronautics, 2018. doi:10.2514/6.2018-0522.

[6] Gern, F., "Improved Aerodynamic Analysis for Hybrid Wing Body Conceptual Design Optimization," *50th AIAA Aerospace*

Sciences Meeting including the New Horizons Forum and Aerospace Exposition, American Institute of Aeronautics and Astronautics, 2012. doi:10.2514/6.2012-249.

[7] Lyu, Z., and Martins, J. R. R. A., "Aerodynamic Design Optimization Studies of a Blended-Wing-Body Aircraft," *Journal of Aircraft*, Vol. 51, No. 5, 2014, pp. 1604–1617. doi:10.2514/1.c032491.

[8] Reist, T. A., and Zingg, D. W., "Aerodynamic Design of Blended Wing-Body and Lifting-Fuselage Aircraft," *34th AIAA Applied Aerodynamics Conference*, American Institute of Aeronautics and Astronautics, 2016. doi:10.2514/6.2016-3874.

[9] Laughlin, T., Corman, J., and Mavris, D., "A Parametric and Physics-Based Approach to Structural Weight Estimation of the Hybrid Wing Body Aircraft," *51st AIAA Aerospace Sciences Meeting including the New Horizons Forum and Aerospace Exposition*, American Institute of Aeronautics and Astronautics (AIAA), 2013. doi:10.2514/6.2013-1082.

[10] Corman, J. A., and Mavris, D. N., "Characterization of an Aero-Structural Interaction for the Hybrid Wing Body Center Section in Conceptual Phase Structural Sizing," *15th AIAA/ISSMO Multidisciplinary Analysis and Optimization Conference*, American Institute of Aeronautics and Astronautics, 2014. doi:10.2514/6.2014-3159.

[11] Nigam, N., Ayyalasomayajula, S. K., Qi, X., Chen, P. C., and Alonso, J. J., "High-Fidelity Weight Estimation for Aircraft Conceptual Design Optimization," *16th AIAA/ISSMO Multidisciplinary Analysis and Optimization Conference*, American Institute of Aeronautics and Astronautics, 2015. doi:10.2514/6.2015-3360.

[12] Felder, J. L., Brown, G. V., DaeKim, H., and Chu, J., "Turboelectric distributed propulsion in a hybrid wing body aircraft," 2011. URL `https://ntrs.nasa.gov/search.jsp?R=20120000856`.

[13] Thomas, R., Burley, C., and Olson, E., "Hybrid Wing Body Aircraft System Noise Assessment with Propulsion Airframe Aeroacoustic Experiment," *16th AIAA/CEAS Aeroacoustics Conference*, American Institute of Aeronautics and Astronautics (AIAA), 2010. doi:10.2514/6.2010-3913.

[14] Garmendia, D. C., Chakraborty, I., and Mavris, D. N., "Method for Evaluating Electrically Actuated Hybrid Wing–Body Control Surface Layouts," *Journal of Aircraft*, Vol. 52, No. 6, 2015, pp. 1780–1790. doi:10.2514/1.c033061.

[15] Garmendia, D. C., Chakraborty, I., and Mavris, D. N., "Multidisciplinary Approach to Assessing Actuation Power of a Hybrid Wing–Body," *Journal of Aircraft*, Vol. 53, No. 4, 2016, pp. 900–913. doi:10.2514/1.c033390.

[16] Cai, Y., Chakraborty, I., and Mavris, D. N., "Integrated Assessment of Vehicle-level Performance of Novel Aircraft Concepts and Subsystem Architectures in Early Design," *2018 AIAA Aerospace Sciences Meeting*, American Institute of Aeronautics and Astronautics, 2018. doi:10.2514/6.2018-1741.

[17] Raymer, D., *Aircraft Design: A Conceptual Approach, Fifth Edition*, American Institute of Aeronautics and Astronautics, Inc., 2012. doi:10.2514/4.869112.

[18] Mattingly, J. D., Heiser, W. H., and Pratt, D. T., *Aircraft Engine Design, Second Edition*, American Institute of Aeronautics and Astronautics, 2002. doi:10.2514/4.861444.

[19] Heath, S. L., Brooks, T. F., Hutcheson, F. V., Doty, M. J., Bahr, C. J., Hoad, D., Becker, L., Humphreys, W. M., Burley, C. L., and Stead, D., "NASA Hybrid Wing Aircraft Aeroacoustic Test Documentation Report," Tech. rep., NASA Langley Research Center, 2016.

[20] Bonet, J. T., Schellenger, H. G., Rawdon, B. K., Elmer, K. R., Wakayama, S. R., Brown, D. L., and Guo, Y., "Environmentally Responsible Aviation (ERA) Project - N+2 Advanced Vehicle Concepts Study and Conceptual Design of Subscale Test Vehicle (STV) Final Report," Tech. rep., Boeing Research Technology & NASA Dryden Flight Research Center, 2011.

[21] Pitera, D. M., DeHaan, M., Brown, D., Kawai, R. T., Hollowell, S., Camacho, P., Bruns, D., and Rawden, B. K., "Blended Wing Body Concept Development with Open Rotor Engine Intergration," Tech. rep., The Boeing Company & NASA Langley Research Center, 2011.

[22] McCullers, L., "Aircraft configuration optimization including optimized flight profiles," 1984.

[23] Harris, C. D., "NASA Supercritical Airfoils: A Matrix of Family-Related Airfoils," Tech. rep., NASA Langley Research Center, 1990.

[24] *STAR-CCM+ Documentation Version 12.02*, Siemens Product Lifecycle Management Software Inc., 2017.

[25] Drela, M., and Youngren, H., *AVL 3.36 User Primer*, MIT, Feb. 2017.

[26] McCullers, L., *Flight Optimization System, Release 8.11, User's Guide*, NASA Langley Research Center, Hampton, VA 23681-0001, Oct. 2009.

[27] Mavris, D. N., and Schutte, J. S., "Application of Deterministic and Probabilistic System Design Methods and Enhancements of Conceptual Design Tools for ERA," Tech. rep., Georgia Institute of Technology & NASA Langley Research Center, 2016.

[28] Corman, J. A., Weston, N., Friedland, C., Mavris, D. N., and Laughlin, T. W., "A Parametric Multi-Fidelity Approach to Conceptual Airframe Design," *2018 AIAA Modeling and Simulation Technologies Conference*, American Institute of Aeronautics and Astronautics, 2018. doi:10.2514/6.2018-1930.

[29] Chakraborty, I., "Subsystem architecture sizing and analysis for aircraft conceptual design," Ph.D. thesis, Georgia Institute of Technology, 2015. URL `https://smartech.gatech.edu/handle/1853/54427`.

[30] Tong, M. T., and Naylor, B. A., "An Object-Oriented Computer Code for Aircraft Engine Weight Estimation," *Volume 1: Aircraft Engine; Ceramics; Coal, Biomass and Alternative Fuels; Manufacturing, Materials and Metallurgy; Microturbines and Small Turbomachinery*, ASME, 2008. doi:10.1115/gt2008-50062.

[31] Roskam, D. J., *Airplane Design Part V: Component Weight Estimation*, Design, Analysis and Research Corporation (DARcorporation), 1999.

[32] Wells, D. P., Horvath, B. L., and McCullers, L. A., "The Flight Optimization System Weights Estimation Method," Tech. rep., 2017.

[33] Lytle, J., Follen, G., Naiman, C., and Evans, A., "Numerical propulsion system simulation (NPSS) 1999 industry review," 2000.

[34] Kirby, M. R., "A Methodology for Technology Identification, Evaluation, and Selection in Conceptual and Preliminary Aircraft Design," Ph.D. thesis, Georgia Institute of Technology, 2001. URL `https://smartech.gatech.edu/handle/1853/12042`.

[35] *777-200/200ER/-300 Airplane Characteristics for Airport Planning*, Boeing Commercial Airplanes, revision e ed., May 2015.

[36] "Advisory circular AC 150/5300-13A," Online, Feb. 2014. URL `https://www.faa.gov/documentLibrary/media/Advisory_Circular/150-5300-13A-chg1-interactive-201804.pdf`.